AgriEngineering

Article

Comparing Two Methods of Leaf Area Index Estimation for Rice (*Oryza sativa* L.) Using In-Field Spectroradiometric Measurements and Multispectral Satellite Images

Jorge Serrano Reyes [1], José Ulises Jiménez [2], Evelyn Itzel Quirós-McIntire [3,4], Javier E. Sanchez-Galan [4,5,*] and José R. Fábrega [2,4,*]

1 Centro de Producción e Investigaciones Agroindustriales, Universidad Tecnológica de Panamá (UTP), El Dorado P.O. Box 0819-07289, Panama; jorge.serrano@utp.ac.pa
2 Centro de Investigaciones Hidráulicas e Hidrotécnicas, Universidad Tecnológica de Panamá (UTP), El Dorado P.O. Box 0819-07289, Panama; ulises.jimenez@utp.ac.pa
3 Instituto de Investigación Agropecuaria de Panamá (IDIAP), El Coco P.O. Box 500-0519, Panama; evelynitzel26@gmail.com
4 Sistema Nacional de Investigación, SENACYT, Edificio 205, Ciudad del Saber P.O. Box 0816-02852, Panama
5 Facultad de Ingenieria de Sistemas Computacionales, Universidad Tecnológica de Panamá (UTP), El Dorado P.O. Box 0819-07289, Panama
* Correspondence: javier.sanchezgalan@utp.ac.pa (J.E.S.-G.); jose.fabrega@utp.ac.pa (J.R.F.); Tel.: +507-560-3933 (J.E.S.-G.); +507-560-3761 (J.R.F.)

Abstract: This work presents a remote sensing application to estimate the leaf area index (LAI) in two rice (*Oryza sativa* L.) varieties (IDIAP 52-05 and IDIAP FL 137-11), as a proxy for crop performance. In-field, homogeneous spectroradiometric measurements (350–1050 nm) were carried in two campaigns (June–November 2017 and January–March 2018), on a private farm, TESKO, located in Juan Hombrón, Coclé Province, Panama. The spectral fingerprint of IDIAP 52-05 plants was collected in four dates (47, 67, 82 and 116 days after sowing), according to known phenological stages of rice plant growth. Moreover, true LAI or green leaf area was measured from representative plants and compared to LAI calculated from normalized PlanetScope multi-spectral satellite images (selected according to dates close to the in-field collection). Two distinct estimation models were used to establish the relationships of measured LAI and two vegetational spectral indices (NDVI and MTVI2). The results show that the MTVI2 based model has a slightly higher predictive ability of true LAI (R^2 = 0.92, RMSE = 2.20), than the NDVI model. Furthermore, the satellite images collected were corrected and satellite LAI was contrasted with true LAI, achieving in average 18% for Model 2 for MTVI2, with the NDVI (Model 1) corrected model having a smaller error around 13%. This work provides an important advance in precision agriculture, specifically in the monitoring of total crop growth via LAI for rice crops in the Republic of Panama.

Keywords: rice crops; phenology; crop performance; leaf area index; Panama; reflectance; remote sensing

Citation: Serrano Reyes, J.; Jiménez, J.U.; Quirós-McIntire, E.I.; Sanchez-Galan, J.E.; Fabrega, J.R. Comparing Two Methods of Leaf Area Index Estimation for Rice (*Oryza sativa* L.) Using In-Field Spectroradiometric Measurements and Multispectral Satellite Images. *AgriEngineering* **2023**, *5*, 965–981. https://doi.org/10.3390/agriengineering5020060

Academic Editors: Murali Krishna Gumma and Travis Esau

Received: 23 December 2022
Revised: 20 May 2023
Accepted: 21 May 2023
Published: 29 May 2023

1. Introduction

Rice (*Oryza sativa* L.) is an essential grain in the primary diet of many people worldwide, especially for inhabitants of developing countries [1]. About 23% of the calories consumed by the world's population come from rice [2]. Rice is mostly produced and consumed within the Asian continent. This continent is also responsible for more than 90% of its world production [2]. In Panama, rice was declared an essential crop for food security, through Law 17 of 22 February 2018 , as this is the main product of the basic food basket in the country (Official Gazette No. 28471-B).

In general, information technology, specially the use of machine learning and big data in agriculture allows the acquisition of quantitative information on crops. It often focuses in

aspects such as location, extension, spatial distribution, monitoring of plants phenological, health, nutritional and water stress status [3,4]. Only with reliable and timely information is it possible to make good crop planning and management decisions. Decisions that at the same time ensure the competitiveness and sustainability of the agricultural sector [5].

Due to its role in food security, rice cultivation, monitoring, and production are in constant technological improvement. Methodologies used for its monitoring often involves remote sensing techniques. For instance, satellite images are used to obtain spectral signatures of vegetation covers [6,7] and reflectance measurements to calculate spectral indices. More importantly, estimating the relationship of these indices against real in-field measured agronomic and biophysical variables is of great interest to the research community [8,9].

A crop's unique spectral signature is fundamental for recognizing vegetation covers. It can be easily described as how a given land cover responds at different wavelengths. Hence, for the realization of crop studies with remote sensing techniques, it is essential to start by obtaining spectral signatures [10]. Often reflectance measurements are used to develop spectral indices, for example: the StandardIzed Difference Vegetation Index (NDVI) [11]; the Soil-Adjusted Vegetation Index (SAVI) [12]; and the Modified Triangular Vegetation Index 2 (MTVI2) [13]. These vegetation spectral indices are quantitative measures calculated from combinations of several spectral bands. They are used to study or indicate vegetation vigor and can be used when studying plots and their changes over time. More importantly, they are more informative and show better sensitivity than individual bands for green vegetation detection [14]. Some vegetation indices can be related to leaf area, biomass, nitrogen content, chlorophyll content, and health status. In this sense, some studies seek to demonstrate and model these relationships to describe crop productivity. Therefore, these vegetation spectral indices are also used to evaluate the correlation level of these with particular crop properties [15–21].

Regarding vegetation indices, the works of Liang et al. [18] and Cao et al. [15] are relevant. In both studies, 443 vegetation indices were evaluated for different characteristics and crops. While Liang et al. [18] uses the leaf area index (LAI) for various crops (especially corn, oats, and potatoes) as a feature to be evaluated, Cao et al. [15] concentrates on the nitrogen content in rice leaves. Other relevant studies are Kross et al. [17] for maize/soybeans and Xie et al. [20] for wheat. It is important to note that the study by Kross et al. [17], also relates the amount of biomass to vegetation indices.

The Leaf Area Index, or LAI, is the ratio between the area of the green leaves and the area of soil. The LAI indicates productivity and photosynthetic capacity [13,22–24]. It is also used to establish growth rates relative to the rate of change concerning incorporating some nutrients [25]. Likewise, other parameters related to LAI were measured, such as the foliar area ratio, which relates the leaf area and the dry mass generated, and the net assimilation rate that evaluates photosynthetic efficiency accounting for dry mass, leaf area, and time [25].

One of the most commonly employed methods for LAI calculation, is the optical method. It calculates LAI as the horizontal shadow area that is projected under a horizontal sheet [26]. Examples of this method are observed in commercial equipment such as the AccuPAR ceptometer and the LAI-2000 Licor. This method has the disadvantage of underestimation due to a saturation phenomenon. A problem can arise with ceptometers at the measurement point [27]. An example of its use is the work of Mora et al. [28], who developed a model to estimate the LAI of the tropical rainforest (*sensu* Holdridge) from spectral data from satellite images, which were validated using field measurements with the *AccuPAR LP-80 ceptometer*.

For the prediction of LAI in rice crops, using multispectral data, it has been suggested to use up to 15 spectral bands [29]. Information from these bands can be applied to inspection, control, and surveillance of extensive rice crops. For example, He et al. [30] studied the effect of panicle presence on LAI estimation for monitoring rice cultivation at the harvest stage.

This article analyzes rice cultivation's spectral signature to obtain the bands that best correlate with the LAI and uses two distinct models for its prediction. The purpose of this work is to contribute to knowledge regarding the use of spectral data from satellite images for the estimation of biophysical variables through remote sensing; specifically, it seeks to establish the basis for the development of models that incorporate vegetation indices for the estimation of the leaf area index, which is applied in the description of the state and productivity of rice cultivation, using *PlanetScope* images.

2. Materials and Methods

2.1. Characterization of the Study Area

The study site is located on the TESKO S.A. farm, in Juan Hombrónn, Coclé Province, at coordinates 8°19′ N, 80°13′ W, approximately 150 km west of Panama City (see Figure 1 for detailed location).

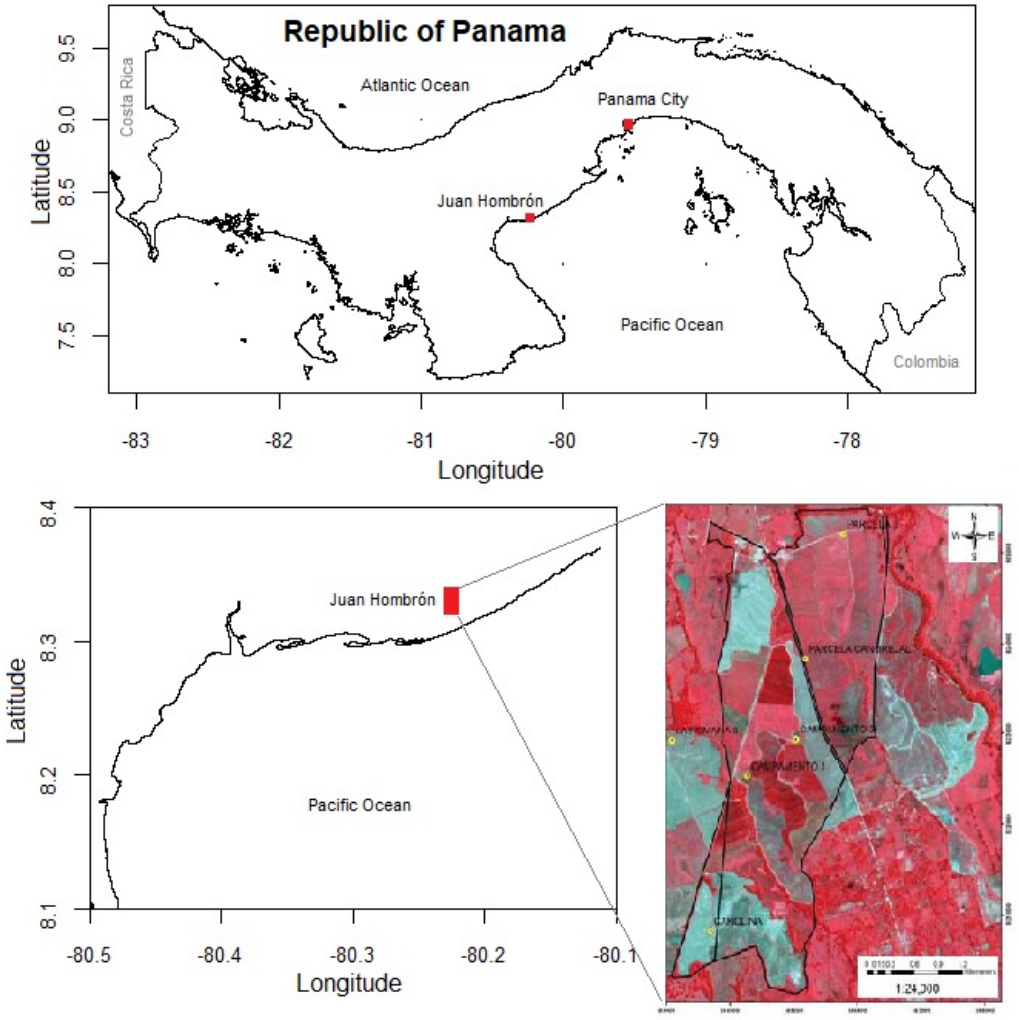

Figure 1. Study site location relative to the Panama City, Panama.

The farm is located in Juan Hombrón, district of Antón, province of Coclé. This location is part of the *Dry Arc* region (the Central Pacific Hydrologic Region of Panama). This region has an average precipitation of 1400 mm per year, in which dry months precipitation could be as low 10 mm/month and in wetmonths up to 500 mm/month [31]. According to Köppen, this region is considered to have a dry-humid tropical climate or tropical Savannah climate. Juan Hombrón's has an economy based on agricultural activities, with

agri-businesses focusing on crops such as: Sugar cane, coffee, corn, rice, beans. In addition, fishing, shrimp farming and livestock are grown in this area.

Cultivar Selection

Originally, IDIAP 52-05 variety was chosen for all experiments in this study due to having a good milling performance and a superior industrial quality. IDIAP 52-05 fulfills its life cycle between 116–124 days after sowing. Plants reach maximum heights of between 85–110 cm and are adapted to both irrigation and rain-fed conditions. More importantly, it is known to be resistant to *Pyricularia* sp. among other pathogens [32].

Therefore, the base unit of analysis for this study were crops of the rice variety IDIAP 52-05 grown on the TESKO S.A. farm. However, it should be stated that management decisions made by the owners of the farm and therefore out out of our hands, impacted the course of this research project and forced the group to use IDIAP 137-11, a similar rice variety to IDIAP 52-05, in order to validate the results. The IDIAP FL 137-11 variety has an early-intermediate vegetative cycle, with 107 to 129 days from sowing under rainfed conditions and 108 to 114 days under irrigated conditions. It has a height that oscillates between 83 and 114 cm [33]. This is of important to establish, since IDIAP FL 137-11 crop with 77 days after sowing, was used for validation of the models.

2.2. Sampling Dates

Rice crops are often divided by the stage in their growth phase. In literature, rice phenology is divided into three main phenological phases (as described in [33,34]), as follows:

- *Phase #1:* vegetative, characterized by starting with germination and concluding with panicle initiation (days 1 to 55 after sowing).
- *Phase #2:* reproductive, characterized by panicle initiation and concluding in flowering (days 55 to 105 after sowing).
- *Phase #3:* maturity or ripening, which is characterized by grain filling and extending until maturity (days 105 to 120 after sowing).

As the rice variety under study develops for about 4 months. The sampling dates, were observed to line up with phenological stages, as follows: (1) vegetative, with a sampling date 47 days after sowing, (2) reproductive with with two sampling dates 67 and 82 days after sowing and (3) maturity with a sampling date 116 days after sowing. This linking is necessary in order to explain their evolution according to management operations for rice crops.

It should be noted that spectral signature at the beginning of the crop on the early vegetative stage (13 days after sowing) were collected. However, as this spectral signatures suffer from suffering from having a mayor reflectance component coming from the soil (due to small leaf area). Measurements of this type are described in length in Sanchez-Galan et al. [35,36]).

2.3. In-Field Spectral Signature Collection

For the capture of spectral signature data, preferential sampling was chosen. That is, taking several replicas of the spectral signature of the coverage class previously identified at homogeneous points, which characterize and represent that class. A spectroradiometer (GER 1500 from Spectra Vista Corporation) covering a range of 350–1050 nm was used, with a field of view of 8°. Before each signature shot, a reference measurement is captured on a *Spectralon* (a calibrated white semi-Lambertian surface). Figure 2 visually represents the team acquiring a in-field with portable spectroradiometer.

Figure 2. In-field spectral Signature collection.

Spectroradiometric measurements were made between June and September 2017 and between January and April 2018. All measurements were acquired in an specific period of the day, either between 10:00 a.m. and 11:30 a.m. or between 1:00 p.m. and 2:30 p.m. This ensured controlled reflactance variability and signal quality. In all cases, a blank (reference measurement), were taken between samples rapidly as the sunlight and clarity conditions changed appreciably. Each signature measurement was georeferenced using a *Garmin eTrex GPS*. Finally, the data were downloaded as text files with ".asc" extension and saved in specific folders. File names were saved with a code indicating the rice variety and the measurement date.

2.4. Transformation of the On-Site Spectral Signature to a Satellite Spectral Signature

Since the equipment manufacturer adhered to the ISO 80000 standard https://www.iso.org/obp/ui/#iso:std:iso:80000:-7:ed-2:v1:en:en%00 (Last accessed on: 2 May 2023) and provided the measurement in units of $W \times cm^{-2} \times nm^{-1} \times sr^{-1} \times 10^{-10}$, it was necessary to make a transformation of spectral signature given by the spectroradiometer to the ones given by the remote sensor from *PlanetScope*, operated by Planet Labs [37]. The solar irradiance was analyzed after a transformation to $W \times m^{-2}$ for each band used, using the Equations (1) and (2):

$$SI_{band} = \sum_{n=0}^{n=m} \lambda_n \cdot BR \cdot \Omega \cdot \left(10^{-6}\right) \quad (1)$$

$$TI_{band} = \sum_{n=0}^{n=m} \lambda_n \cdot TR \cdot \Omega \cdot \left(10^{-6}\right), \quad (2)$$

where *SI* is solar irradiance, *BR* is blank radiance TI is target irradiance, and TR is target radiance. λ_n corresponds to the wavelengths in *nm* and *m* is the number of wavelengths that the spectroradiometer has within each of the *PlanetScope* satellite bands (ρ = {blue, green, red, and infrared}). Ω corresponds to the solid angle in steradians (*sr*), which is related to the field of view by the Equation (3):

$$\Omega = 2\pi\left(1 - \cos\frac{\alpha}{2}\right) \quad (3)$$

For the particular case the in-field equipment had an $\alpha = 8°$, corresponding to a solid angle of $\Omega = 0.0153$ steradians. Finally, the 10^{-6} factor results from the conversion cm^2 to m^2. Thus, the reflectance of a band ρ is obtained by the relationship shown in Equation (4):

$$\rho_{band} = \frac{\mathrm{TI}}{SI} \quad (4)$$

Moreover, on-site spectral signals were re-calculated to take into account the Relative Spectral Response (RSR) filters, that is, the specific *Planetscope* satellite relative sensitivity to radiance at various parts of the electromagnetic spectrum. Filters were obtained directly from Planetscope website for the Dove Classic Satellite.

As the satellite images used in this study were acquired within the 2017–2018 period. Our images belong to the "Dove classic" instrument. Therefore, the sensitivity files were be obtained from a *PlanetScope* forum https://support.planet.com/hc/en-us/articles/360014290293-Do-you-provide-Relative-Spectral-Response-Curves-RSRs-for-your-satellites- (Last accessed on: 2 May 2023), with the code `0fxx/Dove-Classic_10xx`. The RSRs have a value between 0 to 1 and are unit-less, since they are described relative to the peak response; for out of this case, they are shown in Figure 3.

Equation (5), describes the relationship between the reflectance from the spectroradiometer and the reflectance for each the wavelength of each sensor, including the RSR filter.

$$R_{band} = \frac{\sum(R_i \times RSR_i)}{\sum RSR_i} \quad (5)$$

where R_{band}, is the reflectance at a range of wavelength (e.g., red band). R_i, is the reflectance at a specific wavelength, and RSR_i, it the relative response value at the specific wavelength.

This equation have been successfully used in Melillo et al. [38], Trischenko et al. [39,40] and more importantly in Agapiou et al. for the same GER 1500 Spectra Vista Corp. instrument as used for our measurements [41].

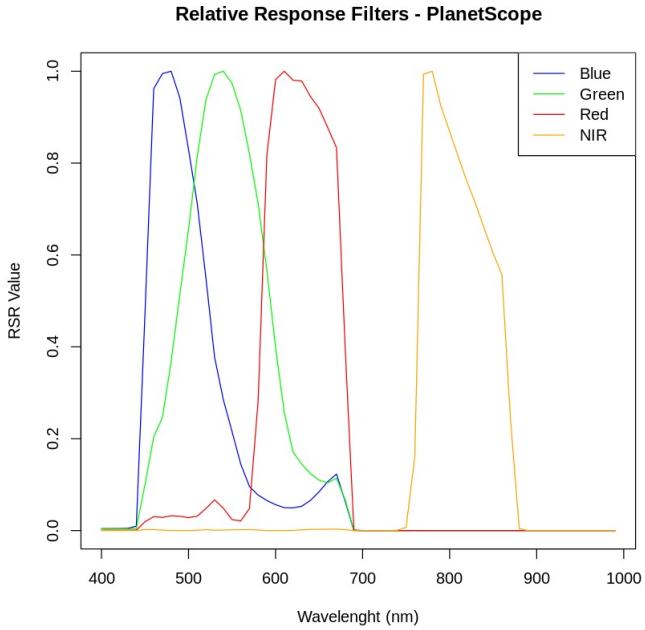

Figure 3. Relative Response filters for ρ_{band} of *PlanetScope* sensor.

2.5. Measurements of Green Leaf Area

Figure 4 shows the process of collection of spectral signatures. In addition, the sampling area selected for True LAI determination. Representative points of the spectral signature of the crop were selected within the plot. Five random samples were cut in triplicate at days 47, 67, 82, 97 and 116; and collected in an area of 25 × 25 cm^2 for the complete cultivation cycle (about 4 months). As demonstrated in Figure 4A, the sampling process consisted of cutting the plant's entire aerial sample with scissors and placing it in a closed bag. As shown in Figure 4B the sampling area was separated with a wooden stick frames and threads, for consistency and repeatability.

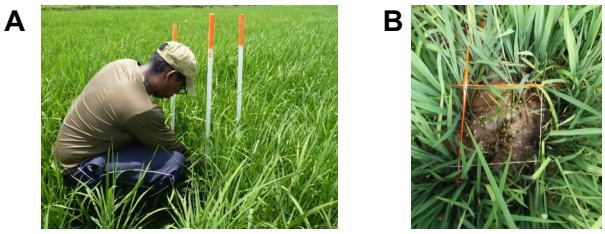

Figure 4. In-field Collection Procedures of Green Leaf Area. Sampling Process (**A**) and Sampling Area (**B**).

Samples collected over the experimental area were taken to the laboratory to estimate the *green leaf area* (dried leaves were not included for the calculation of the area). For this study, this measurement is considered as *true LAI*. Then, each rice leaf was mounted on a flat white cardboard surface, taking into consideration a proportional separation between samples. A calibrated ruler was placed on the cardboard and used as a standard to have the profile object of known dimensions used later for comparison with the leaves. Finally, the mounted leaves were photographed from the top, and the image was saved accordingly for later estimation.

The photographs were analyzed with the *ImageJ program version 1.51t* by selecting a mask to obtain the borders of the leaf finally the shaded area corresponding to the leaf area was calculated [42]. This procedure was repeated twice for selected crop dates. Figure 5, provides a visual explanation of the measurement procedure.

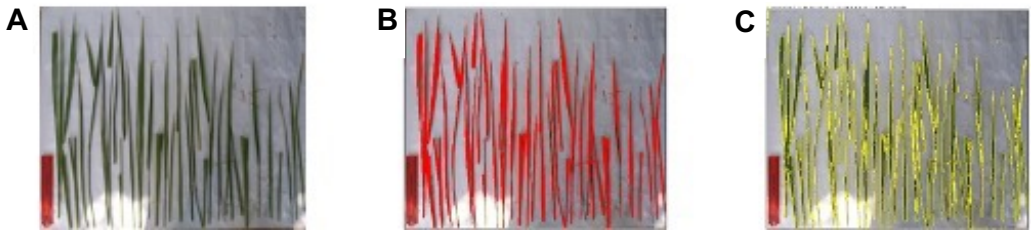

Figure 5. True LAI Determination via the ImageJ software. Leafs were arranged in the controlled background surface (**A**), then the reference and the green leafs were selected and highlighted area confirmed in the software interface (**B**). Finally, the green area was calculated (**C**).

2.6. Modeling the Relationship between In-Situ Reflectance and LAI

Regarding multispectral satellite imagery, *PlanetScope* images were selected, as previously agreed with the funding agency. Selected images had a 3 × 3 m resolution. The satellite bands used in this study were: ρ_{blue} = 455–515 nm, ρ_{green} = 500–590 nm, ρ_{red} = 590–670 nm and ρ_{NIR} = 780–860 nm., respectively. Using the image search engine of *Planet Labs*, a private company that processes and distributes Satellite Images *PlanetScope*, images were identified, selected, and downloaded according to the georeferenced points. Each image was actually a folder with three images. Images that in their name include the suffix "_SR" have radiometric and atmospheric corrections.

These georeferenced satellite images needed to match two criteria: (1) to be in dates as close as possible so that they corresponded to the age of rice cultivation (in days) and (2) those with the lowest percentage of cloud cover. If the captured image did not coincide with the date of measurement in the field or had a significant cloud percentage (as is typical for Panama), images of the nearest day in the same week for the age of the crop were downloaded. These caused a partial time discrepancy between field measurements and satellite acquisition date.

Regarding the images' quality, they all have atmospheric corrections to obtain the ground-level reflectance (surface reflectance). All images used had two predetermined corrections made by the supplier: *atmospheric correction algorithm*: "6Sv2.1" and *aerosol model*: "continental".

2.7. Spectral Estimation of LAI

Two models were used to understand the relationship between true LAI and in-situ reflectance during the vegetative and reproductive phases. Model #1 is directly related to NDVI and Model #2 with the MTVI2. Both, Models #1 and Model #2, were first estimated using Equations (6)–(8), found in literature. Model 1 was first suggested by Nguyen et al. [43] and Model 2 by Haboundane et al. [13], but later estimated to fit the acquired data.

Model # 1

$$LAI = (3.49 \cdot NDVI) - 0.17 \tag{6}$$

where

$$NDVI = \frac{(\rho_{NIR} - \rho_{RED})}{(\rho_{NIR} + \rho_{RED})} \tag{7}$$

Model # 2

$$MTVI2 = \frac{1.5\left[1.2(\rho_{NIR} - \rho_{GREEN}) - 2.5\left(\rho_{RED} - \rho_{green}\right)\right]}{\sqrt{(2\rho_{NIR}+1)^2 - \left(6\rho_{NIR} - \sqrt[5]{\rho_{RED}}\right) - 0.5}} \tag{8}$$

Model validation was made by adding, for all points considered, the percentual errors, by using Equation (9):

$$\left|\frac{\text{true value} - \text{calculated value}}{\text{true value}}\right| \times 100\ (\%) \tag{9}$$

where the true value is represented by the True LAI and the calculated value is the one estimated by each model.

2.8. Calibration Adjustment to PlanetScope Satellite Imagery

Additional radiometric calibration settings were employed relative to initial corrections and referenced to the irradiance and reflectance measured in the field (as a function of the day and time). In other words, the measured in-field spectra were the best approximation of the spectral signature with the slightest error due to the intervention of cloud reflection or infrared re-absorption. The correction factor is the ratio of the field reflectance to the satellite reflectance using the band ranges delimited by the *PlanetScope* sensors.

The correction factor was obtained with the data of four different days from Juan Hombrón plot:

1. 25 January 2018 (field and satellite measurement).
2. 8 February 2018 (field and satellite measurement).
3. 21 February 2018 (only field measurement, satellite measurement was acquired on 22 February 2018).
4. 5 March 2018 (field and satellite measurement)

Figure 6 shows the satellite image from Juan Hombrón plot from which the correction factor was obtained.

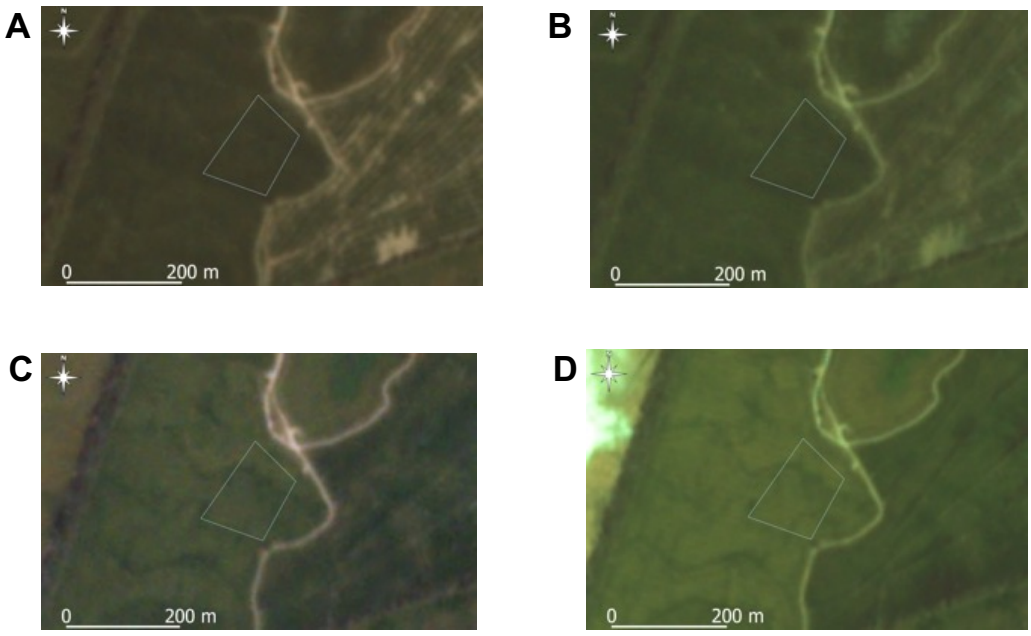

Figure 6. Plots from which correction factor were estimated by date. 25 January 2018 (**A**). 8 February 2018 (**B**), 22 February 2018 (**C**) and 5 March 2018 (**D**).

For all four days the correction factor was estimated as the ratio given in Equation (10):

$$\text{Correction factor} = \frac{\text{field reflectance}}{\text{satellite reflectance}} \tag{10}$$

A correction factor regression with solar irradiance $\frac{\text{W}}{\text{m}^2}$ per band was performed to determine the change in correction factor due to changes in solar irradiance. Finally, reflectance is calculated using Equation (11):

$$\text{Corrected reflectance} = \text{satellite reflectance} \times \text{correction factor} \tag{11}$$

2.9. Software

All satellite imagery was processed with the *QGIS 3.10* software Package [44]. The R program was used for the statistical analysis of data [45], including spectral band integration and figure creation. Statistical significance was established with a cut-off of 0.05 ($p < 0.05$). Second order non-linear polynomial regression needed for calibration betweeen in-field and satellite images were calculated using the *nls* https://cran.r-project.org/web/packages/nls2/index.html (Last accessed on: 2 May 2023) package in R. The Pseudo R^2 estimates for the non-linear regression [46] were calculated using the *aomisc* (https://rdrr.io/github/OnofriAndreaPG/aomisc/ (Last accessed on: 2 May 2023) package from R stastical software.

3. Results

3.1. Analysis of Collected Spectral Signatures

Figure 7 shows the spectral signatures of the IDIAP 52-05 variety for four sampling dates. Figure 7A provides a representation of vegetative phase on day 47 after sowing. Figure 7B,C represents the reproductive phase on days 67 and 82 after sowing, respectively. Figure 7D, shows the maturity phase, specifically on day 116 after sowing. This figure shows the evolution of the spectral signatures over time and, more importantly, its spectral separability. One can notice that the first and last phases have a lower overall reflectance, contrasting with the reproductive having higher reflectance, with notable reflectance attributed to the plant's flowering.

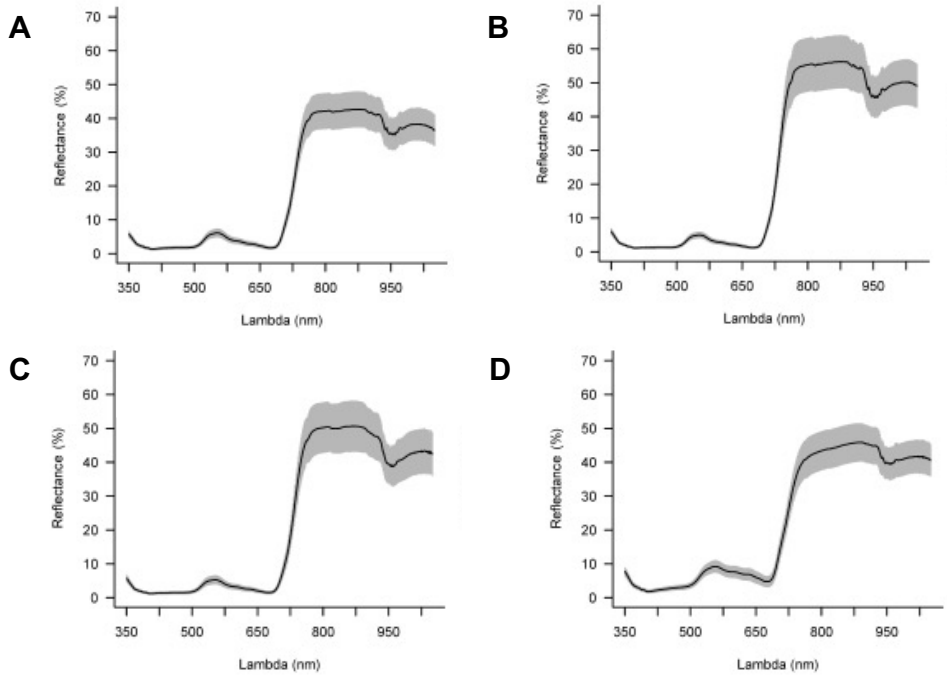

Figure 7. Average spectral signatures for the rice variety IDIAP 52-05. Representative signature for 47 days after sowing, corresponding to 24 May 2017 (**A**). Representative signature with 67 days after sowing, corresponding to 13 June 2017 (**B**). Representative signatures for 82 days after sowing, corresponding to 28 June 2017 (**C**). Finally, Signatures for 116 days after sowing, corresponding to 2 August 2017 (**D**). The black line represents the average, and the gray shading defines the range of ± 1 standard deviation.

3.2. True LAI Estimation

As it was previously described in Section 2.5, true LAI was calculated via image analysis of rice plant leaves. The leaves were cut out, and then the ImageJ program was used to count the green area of the leaves in the photograph scaled with an object of known dimension. Table 1, shows the estimated average true LAI for the IDIAP 52-05 variety at different days after sowing. The Mean Absolute Deviation (MAD) was calculated to assess the dispersion values in LAI measurements for each sowing date. For the calculation of the MAD Equation (12), was used:

$$\text{MAD} = \frac{\sum |x_{ij} - \bar{x}_j|}{n_j} \tag{12}$$

where in x_{ij}, i represents each one of the measurements of j days after sowing, $\bar{x}_j$ is the average for j days after sowing, and n is the total number of samples for the date.

As for the interpretation this value, a low MAD value indicates that the data points are closely together; while a high MAD value indicates their dispersion.

Table 1. True LAI (Green leaf area) estimates for IDIAP 52-05 variety.

Phase	Days after Sowing	Measured LAI	Mean Absolute Deviation for LAI
Vegetative	47	3.48, 4.20, 6.36	1.12
Reproductive	67	5.71, 6.45, 9.33	1.44
	82	5.71, 6.20, 9.36	1.51
Maturity	97	8.25, 9.54, 9.94	0.66
	116	4.00, 4.96, 5.05	0.45

Table 1 suggests that there is more dispersion (higher MAD values) in LAI measurements in the reproductive phase (for 67 and 82 days after sowing) with 1.44 and 1.51,

respectively; than in the vegetative (for 47 days after sowing) with 1.12 and ripening phases (for 97 and 116 days after sowing) with 0.66 and 0.45, respectively.

In general, these variations in LAI measurements for the same collection day can be attributed to the nature of the experiment. As the experiments were carried out on a commercial farm, with particular soil and terrain characteristics. Basically, the terrain was not a flat and well-maintained crop surface, but an even surface where muddy puddles were formed, which led to variations in plant growth. Moreover, as in any commercial farm, the seed planting was performed via a broadcast seeder; therefore, the location of plants is not equally spaced, specially when compared to traditional experimental plots where row planting and drop spreaders/seeders are often used. Finally, it is known that the growth stages for IDIAP 52-05 work as a gradient with some plants changing phases more rapidly than others [33]. These growth variations are reflected in our LAI measurements.

3.3. Model for In-Field Spectral Estimation of LAI

Equations described in Section 2.7 were used to understand the resulting relationship between in-situ reflectance and True LAI in the vegetative and reproductive phases, with n = 52 points averaged into 4 points representing dates after sowing (47, 67, 82 and 97). Model #1, for NDVI, resulted in a significant linear model ($p < 0.05$) with a multiple R-squared of 0.92 and an adjusted R-squared of 0.89, and a RMSE of 2.22. The resulting model can be expressed as $LAI = 8.57 \times NDVI$. As for Model #2, for MTVI2, resulted in a statistically significant linear model ($p < 0.05$) with a multiple R-squared of 0.92 and an adjusted R-squared of 0.89, and a RMSE of 2.20. The resulting model can be expressed as $LAI = 10.45 \times MTVI2$. These results show that the MTVI2 base model has a slightly higher predictive ability of LAI, with a slightly smaller error than the one using NDVI.

3.4. Relative Correction of the Satellite Image

Figure 8 shows, the 2nd order corrections for each band. Table 2 presents the ratio of change between the correction factor against irradiance by satellite band measured with the field spectroradiometer. Table 3 shows correction factor regression with solar irradiance $\frac{W}{m^2}$ per band was performed to determine the change in correction factor due to changes in solar irradiance.

Correction reflectance applied according to Equation (11) earlier for the irradiance of 8 February 2018, suggests a correction of 0.61911 for the Blue Band. While corrections of 0.6121, 0.4058, and 1.355 must be applied to the Green, Red, and NIR Bands, respectively.

Each model was applied on a PlanetScope satellite image to obtain the LAI maps (see Figure 9). The image is from 8 February 2018 and the object of observation was the crop IDIAP FL 137-11.

Table 2. Equations used to calculate the correction factor for the bands used.

Band	Final Model	Residual Standard Error	Signifcance	Pseudo R^2
Blue	$Y = 0.0009 \times x^2 - 0.2127 \times x + 11.92$	0.1005	$p < 0.001$	0.53
Green	$Y = 0.0004 \times x^2 - 0.1568 \times x + 15.09$	0.1739	$p < 0.001$	0.36
Red	$Y = 0.0007 \times x^2 - 0.2506 \times x + 22.46$	0.1485	$p < 0.001$	0.68
NIR	$Y = -0.0004 \times x^2 + 0.1288 \times x - 9.0127$	0.1528	$p < 0.05$	0.41

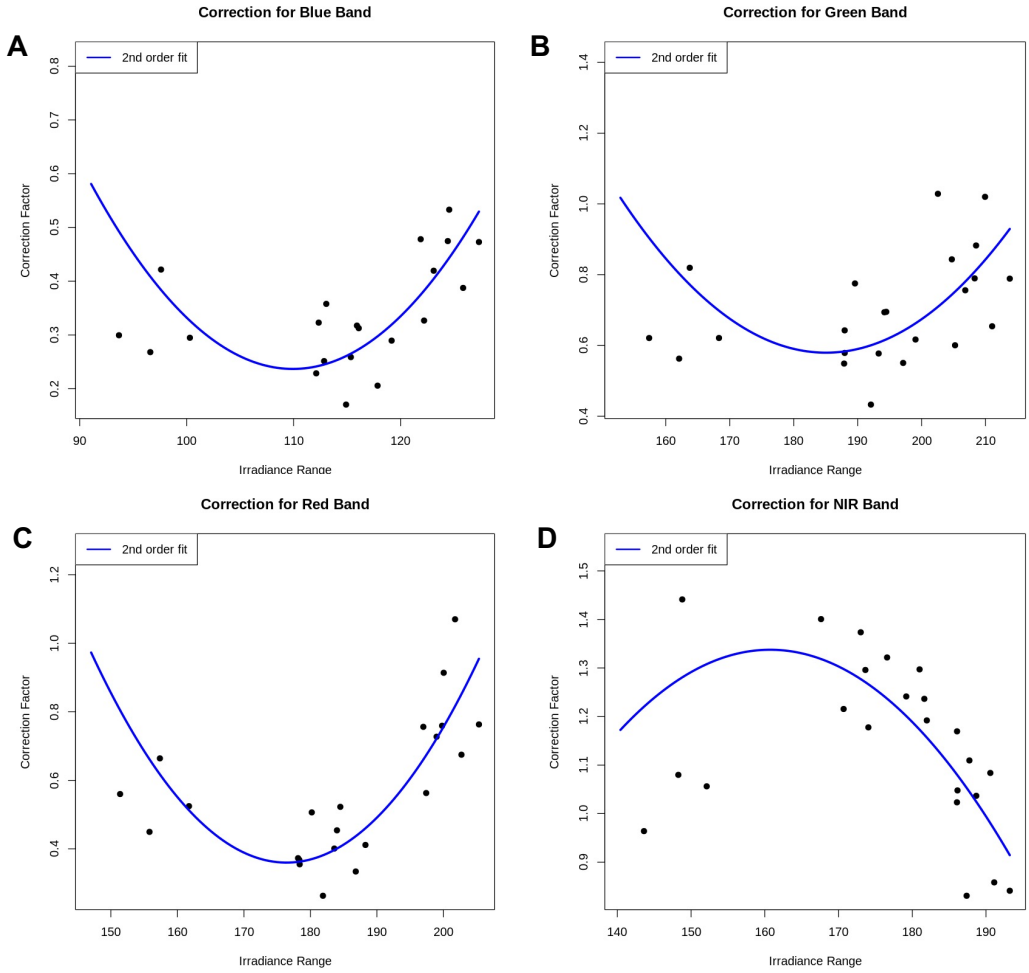

Figure 8. Visual representation of correction factor for the bands.

Table 3. Estimated spectral corrections made using the irradiance for 8 February 2018, by bands.

Sample	Irradiance			
	Blue Band	Green Band	Red Band	NIR Band
1	106.137	177.2489	169.5444	161.3283
2	106.1878	177.241	169.2943	158.1286
3	105.7683	176.4078	168.4679	159.3418
4	104.2549	173.8378	166.0449	159.3632
5	107.4158	179.0375	170.9401	161.7234
6	105.515	175.912	167.9908	160.3049
7	104.5517	174.196	166.2761	158.6433
Average	105.6901	176.2687	168.3655	159.8334

We worked with the exact polygon measured in the field. For this purpose, the coordinates of the points measured in the field were used. The points of the edges and ends were taken in order to form a polygon. The coordinates of the polygon are 4 points as listed below:

1. 920,757.68 N and 584,436.09 E
2. 920,718.36 N and 584,545.32 E
3. 920,822.46 N and 584,602.76 E
4. 920,893.83 N and 584,531.64 E

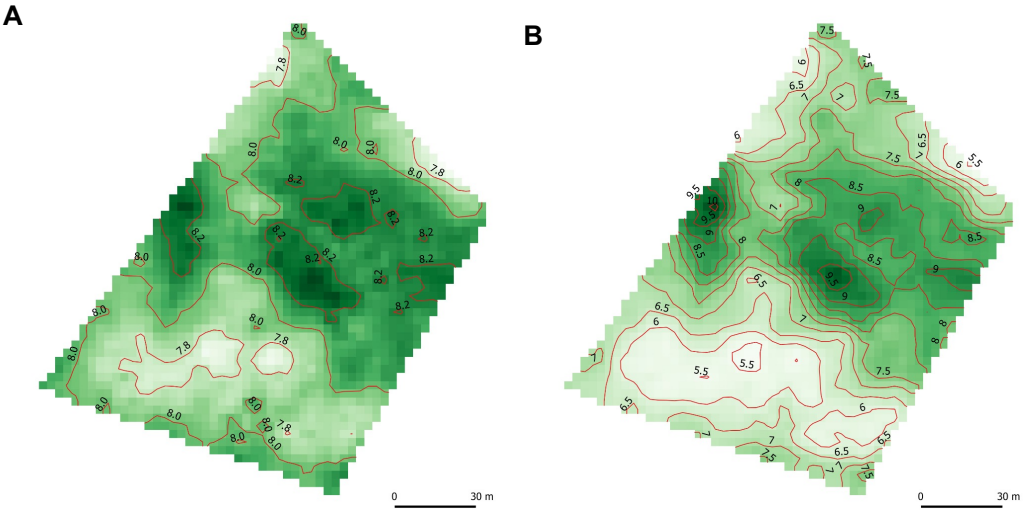

Figure 9. Estimated LAI map from PlanetScope images measured on 8 February 2018. LAI map estimated using model 1 with NDVI (**A**). LAI map estimated using model 2 with MTVI2 (**B**).

3.5. Validating the Satellite Image Correction

Tables 4 and 5 shows the LAI prediction error for Model #1 and Model #2, respectively. For both models the estimated LAI with the *PlanetScope* bands against the true LAI (obtained by cutting leaves) are compared for both models. Estimation from Two LAI measurements was employed for each model.

Table 4. Model #1 Validation and Error Calculation.

Model	Calculated NDVI	Measured LAI	Estimated LAI	Percentual Error (%)
1	0.9189	7.71	8.03	4.15
	0.9164	6.51	8.00	22.09

Table 5. Model #2 Validation and Error Calculation.

Model	Calculated MTVI2	Measured LAI	Estimated LAI	Percentual Error (%)
2	0.8057	7.71	8.41	9.03
	0.8009	6.51	8.35	28.26

Model #1's average percentual error is 13.52%; for Model #2 the error amounted to 18.65%. Both cases required a detailed analysis of the relative correction of the satellite image. This analysis was made to understand further the model and how this error could be reduced.

4. Discussion and Conclusions

Visualizing spectral signatures serves to identify bands that can be used to discriminate between classes. Yang and Chen [47] mention that in the vegetative phase, the signatures are affected by: the change in leaf area, the growth of the leaves in number and size, and the soil discovered; the smaller the leaf area, the greater the interference of the soil discovered in the firm. The spectral response of rice cover crops grown within a few days after sowing showed a constant variation in the reflectance range along the signature. This spectral response does not reach the shape of a typical plant toppings signature. Spectral responses at ages 47, 67, 82, and 116 days after sowing show the typical distinctive features of vegetation: low reflectance in the visible light range, a noticeable peak in the green around 570 nm, and high near-infrared reflectivity [10].

With the plant's growth, an average increase in reflectivity is observed in the near-infrared, but the variability in this band is high, suggesting difficulty in detectability. The

variation in the near-infrared range is likely due to differences in the water content in the plant's leaves [10].

The reflectance was higher at 67–82 days after sowing (which comprises 2 phases, the final days of the reproductive phase and the beginning of the ripening phase) compared to the other sowing dates, which coincides with the results of [48], in tests performed on the *Kongyu* rice variety in China. The presence of the panicle also increases reflectance in the near-infrared range, which is consistent with the results of He et al. [30] for the *japonica* rice variety. At 116 days after sowing (last stages of cultivation), a decay of reflectance is observed, possibly due to decreased leaf water content and the loss of green leaf area.

Relative to the LAI, each true LAI value resulted from averaging three measures of LAI for each planting age. In the measurements of true LAI of the variety IDIAP 52-05 it is observed that the samples of an area of 25 $\times$ 25 cm^2 present high variability especially at the older age of the crop.

As for the treatment of the images, these are acquired with a correction that estimates the reflectance at the level of the Earth's surface [35]; which consists of the application of the standard atmospheric correction that is made with the algorithm 6S version 2.1, with continental aerosol content model and optical thickness data provided by MODIS satellite images [49]. The atmospheric correction methodology applied to *PlanetScope* products has some limitations such as needing overlap with areas measured with the MODIS satellite and the lack of correction in the presence of thin clouds or mist [49]. The additional correction factor brings the measurement of PlanetScope's corrected product at a ground level closer to the direct reflectivity measurement with the spectroradiometer. The correction factor is not static and varies between bands as it can be seen in Table 3. When comparing the Measured LAI for the verification points shown in Tables 4 and 5 to the average spectral signature of plants with the same days after sowing (with in-field measurements and those shown in Table 1) it seems plausible and very well in range with a plant with 77 days with 7.71 and 6.51, respectively, thus a verification of the procedure.

This work applied individual band correction factors to the satellite images. For all bands, a quadratic model was fitted. The correction factor tended to decrease to a minimum of irradiance defined for each band with values of 110 (blue), 185 (green), and 175 (red), and then increase. For the case of the NIR band, the behavior of the correction factor was precisely the opposite, showing an increase to a maximum irradiance of 160. Then a decrease in IR band. Table 2 shows the correction equations used for each band and the irradiance range applicable to the theme represented.

The validation test performed using two measurements of true LAI of the IDIAP FL 137-11 crop 77 days after sowing determined that model 1 presented an error rate of 13.52% comparing the estimated and true LAI values. Model 2 with MTVI2 obtained a predictive approximation with a 18.65% error. In general, literature shows that MTVI2 has a higher correlation rate with LAI for corn, soybeans, and wheat and less sensitivity to chlorophyll variations [13], such as rice in the ripening phases.

More importantly, the average magnitude of the errors for both Model #1 and Model #2 is around 15%, it can be attributed to many factors, but it can be accounted to the uneven distribution of LAI values. In fact, the maps shown on Figure 9 show that LAI estimates on the images form big homogeneous groups for Model #1 and small heterogeneous groups for Model #2. These notable distribution differences might be due to irregularities at the ground level, a byproduct of the experiment being performed on a commercial farm instead of an experimental plot. In addition, errors of estimated LAI around 20% are most likely due to other limitations of this study, such as the inevitable change in rice varieties, differences in the soil, and the seasonal difference between collection and validation dates. That are mostly noted by points having the same LAI, but changing significantly in the in-field spectral signatures in the NIR bands. In addition, different LAI values for similar NIR band values.

Despite limitations, and the fact that the resulting fitted models (and their results here presented), are only valid for *PlanetScope* satellite images, since they were adjusted to

the bandwidths and sensitivity of *PlanetScope Dove classic* equipment. This work provides an important advance in precision agriculture, specifically in monitoring LAI for rice crops. The LAI is a physical parameter closely related to productivity and key to applying the various models employed, including the one related to MTVI2, allowing predictions consistent with the real LAI using *PlanetScope* satellite imagery.

Author Contributions: Conceptualization, J.S.R., E.I.Q.-M., J.U.J., J.E.S.-G. and J.R.F.; methodology, J.S.R., E.I.Q.-M., J.U.J., J.E.S.-G. and J.R.F.; software, J.S.R. and J.U.J.; validation, J.S.R., E.I.Q.-M., J.U.J., J.E.S.-G. and J.R.F.; resources, E.I.Q.-M. and J.R.F.; writing—original draft preparation, J.S.R., J.U.J., J.E.S.-G. and J.R.F.; writing—review and editing, J.S.R., E.I.Q.-M., J.U.J., J.E.S.-G. and J.R.F.; visualization, J.S.R. and J.U.J.; supervision of students, J.R.F. and E.I.Q.-M. All authors have read and agreed to the published version of the manuscript.

Funding: J.S.R. was supported by a scholarship of the *Programa de Fortalecimiento de los Postgrados Nacionales* from the National Secretariat for Science, Technology and Innovation (SENACYT). This work was supported by SENACYT through the project "Design of an expert system based on spectral signatures of agricultural coverage in Panama" (IDDS 15-184). E.I.Q.-M., J.E.S.-G. and J.R.F. are suppported by the Sistema Nacional de Investigacion (SNI) of SENACYT.

Data Availability Statement: In-field spectroscopical data collected is available upon request.

Acknowledgments: The authors acknowledge administrative support provided by the Universidad Tecnológica de Panamá and IDIAP El Coco.

Conflicts of Interest: The authors declare no conflict of interest.

References

1. Farahzadi, F.; Ebrahimi, A.; Zarrinnia, V.; Azizinezhad, R. Evaluation of Genetic Diversity in Iranian Rice (*Oryza sativa*) Cultivars for Resistance to Blast Disease Using Microsatellite (SSR) Markers. *Agric. Res.* **2020**, *9*, 460–468. [CrossRef]
2. Sharma, T.R.; Rai, A.K.; Gupta, S.K.; Vijayan, J.; Devanna, B.N.; Ray, S. Rice Blast Management Through Host-Plant Resistance: Retrospect and Prospects. *Agric. Res.* **2012**, *1*, 37–52. [CrossRef]
3. Osinga, S.A.; Paudel, D.; Mouzakitis, S.A.; Athanasiadis, I.N. Big data in agriculture: Between opportunity and solution. *Agric. Syst.* **2022**, *195*, 103298. [CrossRef]
4. Cravero, A.; Pardo, S.; Sepúlveda, S.; Mu noz, L. Challenges to Use Machine Learning in Agricultural Big Data: A Systematic Literature Review. *Agronomy* **2022**, *12*, 748. [CrossRef]
5. García, S.A.; Martínez, L.J. Método para identificación de cultivos de arroz (*Oryza sativa* L.) con base en imágenes de satélite. *Agron. Colomb.* **2010**, *38*, 281–290.
6. Xu, T.; Wang, F.; Yi, Q.; Xie, L.; Yao, X. A Bibliometric and Visualized Analysis of Research Progress and Trends in Rice Remote Sensing over the Past 42 Years (1980–2021). *Remote Sens.* **2022**, *14*, 3607. [CrossRef]
7. Zheng, J.; Song, X.; Yang, G.; Du, X.; Mei, X.; Yang, X. Remote sensing monitoring of rice and wheat canopy nitrogen: A review. *Remote Sens.* **2022**, *14*, 5712. [CrossRef]
8. Zhou, J.; Lu, X.; Yang, R.; Chen, H.; Wang, Y.; Zhang, Y.; Huang, J.; Liu, F. Developing Novel Rice Yield Index Using UAV Remote Sensing Imagery Fusion Technology. *Drones* **2022**, *6*, 151. [CrossRef]
9. San Bautista, A.; Fita, D.; Franch, B.; Casti neira-Ibá nez, S.; Arizo, P.; Sánchez-Torres, M.J.; Becker-Reshef, I.; Uris, A.; Rubio, C. Crop monitoring strategy based on remote sensing data (Sentinel-2 and Planet), Study case in a rice field after applying Glycinebetaine. *Agronomy* **2022**, *12*, 708. [CrossRef]
10. Chuvieco, E. *Teledetección Ambiental: La Observación de la Tierra Desde el Espacio*; Ariel Ciencias, Editorial Ariel: Barcelona, Spain, 2010.
11. Rouse, J.W.; Haas, R.W.; Schell, J.A.; Deering, D.W.; Harlan, J.C. Monitoring the Vernal Advancement and Retrogradation (Greenwave Effect) of Natural Vegetation NASA/GSFCT Type III Final Report. 1974. Available online: https://ntrs.nasa.gov/citations/19750020419 (accessed on 17 April 2023).
12. Huete, A. A soil-adjusted vegetation index (SAVI). *Remote Sens. Environ.* **1988**, *25*, 295–309. [CrossRef]
13. Haboudane, D.; Miller, J.R.; Pattey, E.; Zarco-Tejada, P.J.; Strachan, I.B. Hyperspectral vegetation indices and novel algorithms for predicting green LAI of crop canopies: Modeling and validation in the context of precision agriculture. *Remote Sens. Environ.* **2004**, *90*, 337–352. [CrossRef]
14. Bannari, A.; Morin, D.; Bonn, F.; Huete, A.R. A review of vegetation indices. *Remote Sens. Rev.* **1995**, *13*, 95–120. [CrossRef]
15. Cao, Q.; Miao, Y.; Shen, J.; Yu, W.; Yuan, F.; Cheng, S.; Huang, S.; Wang, H.; Yang, W.; Liu, F. Improving in-season estimation of rice yield potential and responsiveness to topdressing nitrogen application with Crop Circle active crop canopy sensor. *Precis. Agric.* **2016**, *17*, 136–154. [CrossRef]

16. Din, M.; Zheng, W.; Rashid, M.; Wang, S.; Shi, Z. Evaluating hyperspectral vegetation indices for leaf area index estimation of *Oryza sativa* L. at diverse phenological stages. *Front. Plant Sci.* **2017**, *8*, 820. [CrossRef]
17. Kross, A.; McNairn, H.; Lapen, D.; Sunohara, M.; Champagne, C. Assessment of RapidEye vegetation indices for estimation of leaf area index and biomass in corn and soybean crops. *Int. J. Appl. Earth Obs. Geoinf.* **2015**, *34*, 235–248. [CrossRef]
18. Liang, L.; Di, L.; Zhang, L.; Deng, M.; Qin, Z.; Zhao, S.; Lin, H. Estimation of crop LAI using hyperspectral vegetation indices and a hybrid inversion method. *Remote Sens. Environ.* **2015**, *165*, 123–134. [CrossRef]
19. Serrano Reyes, J.; Fábrega, J.R.; Quirós-McIntire, E.I.; Sánchez-Galán, J.E.; Jiménez, J.U. Análisis Prospectivo de la Detección Hiperespectral de Cultivos de Arroz (*Oryza Sativa* L.). *KnE Eng.* **2018**, *3*, 69. [CrossRef]
20. Xie, Q.; Huang, W.; Liang, D.; Chen, P.; Wu, C.; Yang, G.; Zhang, J.; Huang, L.; Zhang, D. Leaf area index estimation using vegetation indices derived from airborne hyperspectral images in winter wheat. *IEEE J. Sel. Top. Appl. Earth Obs. Remote Sens.* **2014**, *7*, 3586–3594. [CrossRef]
21. Jiménez, J.U.; Quirós-McIntire, E.I.; Camargo-García, V.; Serrano, J.; Sánchez-Galán, J.; Fábrega, J. Caracterización morfológica y espectral de 6 variedades criollas de arroz (*Oryza sativa* L.) en Panamá. In Proceedings of the Innovation in Education and Inclusion: Proceedings of the 16th LACCEI International Multi-Conference for Engineering, Education and Technology, Lima, Peru, 18–20 July 2018.
22. Monsi, M.; Saeki, T. On the factor light in plant communities and its importance for matter production. *Ann. Bot.* **2005**, *95*, 549. [CrossRef]
23. Yang, Y.; Qiu, J.; Zhang, R.; Huang, S.; Chen, S.; Wang, H.; Luo, J.; Fan, Y. Intercomparison of three two-source energy balance models for partitioning evaporation and transpiration in semiarid climates. *Remote Sens.* **2018**, *10*, 1149. [CrossRef]
24. Colaizzi, P.D.; Kustas, W.P.; Anderson, M.C.; Agam, N.; Tolk, J.A.; Evett, S.R.; Howell, T.A.; Gowda, P.H.; O'Shaughnessy, S.A. Two-source energy balance model estimates of evapotranspiration using component and composite surface temperatures. *Adv. Water Resour.* **2012**, *50*, 134–151. [CrossRef]
25. Jarma, A.d.J.; Degiovanni, V.M.; Montoya, R.A. Índices fisiotécnicos, fases de crecimiento y etapas de desarrollo de la planta de arroz. In *Producción Eco-Eficiente del Arroz en América Latina. Publicación CIAT No. 365*; Degiovanni, B.V., Martínez, R.C.P., Motta, O.F., Eds.; Centro Internacional de Agricultura Tropical (CIAT): Cali, Colombia, 2010; Chapter 5, Volume Tomo I, 487p.
26. Ross, J. The radiation Regime and Architecture of Plant Stands. *Tasks Veg. Sci.* **1981**, *3*, 391. [CrossRef]
27. Casa, R.; Upreti, D.; Pelosi, F. Measurement and estimation of leaf area index (LAI) using commercial instruments and smartphone-based systems. *IOP Conf. Ser. Earth Environ. Sci.* **2019**, *275*, 012006. [CrossRef]
28. Mora, D.; Jiménez, J.U.; Fábrega, J.R. Relación Entre el Índice de Área Foliar y el Índice Normalizado de Vegetación en el Bosque Húmedo Tropical de Panamá en Gamboa. *I + D Tecnológico* **2014**, *10*, 28–40.
29. Wang, F.m.; Huang, J.f.; Lou, Z.h. A comparison of three methods for estimating leaf area index of paddy rice from optimal hyperspectral bands. *Precis. Agric.* **2011**, *12*, 439–447. [CrossRef]
30. He, J.; Qin, Y.; Guo, C.; Zhao, L.; Zhou, X.; Yao, X.; Cheng, T.; Tian, Y. Monitoring leaf area index after heading stage using hyperspectral remote sensing data in rice. In Proceedings of the 2016 IEEE International Geoscience and Remote Sensing Symposium (IGARSS), Beijing, China, 10–15 July 2016; IEEE: Piscataway, NJ, USA, 2016; pp. 6284–6287. [CrossRef]
31. Castrellón, M.G.; Pauloo, R.A.; Popescu, I.; Fábrega, J. ONASP: A web application for groundwater data visualization in Panama. *IOP Conf. Ser. Earth Environ. Sci.* **2023**, *1136*, 012028. [CrossRef]
32. Buitrago, I.C. *Las Variedades Mejoradas de Arroz del Idiap: Un Aporte al Desarrollo del Sector Arrocero Panameño 1975–2010*; Instituto de Investigación Agropecuaria de Panamá, Departamento de Ediciones y Publicaciones: Panama City, Panama, 2012.
33. Buitrago, I.C.; Quirós McIntire, E.I.; Zachrisson Salamina, B. *Fenología de la Planta de Arroz y su Importancia en el Manejo Integrado del Cultivo*; Instituto de Investigación Agropecuaria de Panamá, Departamento de Ediciones y Publicaciones: Panama City, Panama, 2012.
34. Ariza, A.A. Machine Learning and Big Data Techniques for Satellite-Based Rice Phenology Monitoring. Master's Thesis, The University of Manchester, Manchester, UK, 2019.
35. Sánchez-Galán, J.E.; Serrano Reyes, J.; Jiménez, J.U.; Quirós-McIntire, E.I.; Fábrega, J.R. Supervised Classification of Spectral Signatures from Agricultural Land-Cover in Panama Using the Spectral Angle Mapper Algorithm. In Proceedings of the 2019 XLV Latin American Computing Conference (CLEI), Panama City, Panama, 30 September–4 October 2019; IEEE: Piscataway, NJ, USA, 2019. [CrossRef]
36. Sánchez-Galán, J.E.; Barranco, F.R.; Reyes, J.S.; Quirós-McIntire, E.I.; Jiménez, J.U.; Fábrega, J.R. Using Supervised Classification Methods for the Analysis of Multi-spectral Signatures of Rice Varieties in Panama. *Adv. Sci. Technol. Eng. Syst. J.* **2021**, *6*, 552–558. [CrossRef]
37. Planet Labs Inc. *Planet Imagery Product Specifications*; Planet Labs Inc.: San Francisco, CA, USA, 2021. Available online: https://assets.planet.com/docs/Combined-Imagery-Product-Spec-Dec-2018.pdf (accessed on 26 April 2023).
38. Melillos, G.; Hadjimitsis, D.G. Detection Underground Structures in Cyprus Using Landsat-8 Bands. In Proceedings of the IGARSS 2020–2020 IEEE International Geoscience and Remote Sensing Symposium, Waikoloa, HI, USA, 26 September–2 October 2020; IEEE: Piscataway, NJ, USA, 2020; pp. 1181–1184.
39. Trishchenko, A.P.; Cihlar, J.; Li, Z. Effects of spectral response function on surface reflectance and NDVI measured with moderate resolution satellite sensors. *Remote Sens. Environ.* **2002**, *81*, 1–18. [CrossRef]

40. Trishchenko, A.P. Effects of spectral response function on surface reflectance and NDVI measured with moderate resolution satellite sensors: Extension to AVHRR NOAA-17, 18 and METOP-A. *Remote Sens. Environ.* **2009**, *113*, 335–341. [CrossRef]
41. Agapiou, A.; Hadjimitsis, D.G.; Alexakis, D.D. Evaluation of broadband and narrowband vegetation indices for the identification of archaeological crop marks. *Remote Sens.* **2012**, *4*, 3892–3919. [CrossRef]
42. Abramoff, M.D.; Magalhaes, P.J.; Ram, S.J. Image Processing with ImageJ. *Biophotonics Int.* **2004**, *11*, 36–42.
43. Nguyen, H.T.; Lee, B.W. Assessment of rice leaf growth and nitrogen status by hyperspectral canopy reflectance and partial least square regression. *Eur. J. Agron.* **2006**, *24*, 349–356. [CrossRef]
44. QGIS Development Team. QGIS Geographic Information System. Open Source Geospatial Foundation Project. 2020. QGIS Association. Available online: https://www.qgis.org (accessed on 26 April 2023).
45. R Core Team. *R: A Language and Environment for Statistical Computing*; R Foundation for Statistical Computing: Vienna, Austria, 2020.
46. Spiess, A.N.; Neumeyer, N. An evaluation of R2 as an inadequate measure for nonlinear models in pharmacological and biochemical research: A Monte Carlo approach. *BMC Pharmacol.* **2010**, *10*, 6. [CrossRef] [PubMed]
47. Yang, C.M.; Chen, R.K. Modeling rice growth with hyperspectral reflectance data. *Crop Sci.* **2004**, *44*, 1283–1290. [CrossRef]
48. Gnyp, M.L.; Miao, Y.; Yuan, F.; Ustin, S.L.; Yu, K.; Yao, Y.; Huang, S.; Bareth, G. Hyperspectral canopy sensing of paddy rice aboveground biomass at different growth stages. *Field Crop. Res.* **2014**, *155*, 42–55. [CrossRef]
49. Collison, A.; Wilson, N. *Planet Surface Reflectance Product*; Version 1.0.; Planet Labs, Inc.: San Francisco, CA, USA, 2018.